Temperature dependence of island growth shapes during submonolayer deposition of Ag on Ag(111)

Erik Cox,[1] Maozhi Li,[2,*] Po-Wen Chung,[1] C. Ghosh,[2] T. S. Rahman,[3] C. J. Jenks,[1] J. W. Evans,[4] and P. A. Thiel[1]
[1]*Department of Chemistry and Ames Laboratory, Iowa State University, Ames, Iowa 50011, USA*
[2]*Institute of Physical Research and Technology and Ames Laboratory, Iowa State University, Ames, Iowa 50011, USA*
[3]*Department of Physics, Kansas State University, Manhattan, Kansas 66506, USA*
[4]*Department of Mathematics and Ames Laboratory, Iowa State University, Ames, Iowa 50011, USA*
(Received 22 September 2004; revised manuscript received 17 December 2004; published 15 March 2005)

Growth shapes of Ag islands formed on Ag(111) during submonolayer deposition at different temperatures were studied with scanning tunneling microscopy, and analyzed via kinetic Monte Carlo simulation of a suitable atomistic lattice-gas model. Distinct shape transitions can be observed, from dendrites with triangular envelopes at low temperatures (below 140 K) to more isotropic fat fractal islands at intermediate temperatures, and then to distorted hexagonal shapes with longer *B* steps and shorter *A* steps at higher temperatures (above 170 K). In contrast, the equilibrium island shapes in this system are almost perfect hexagons displaying a near-sixfold symmetry. Modeling reveals that the broken symmetry of growth shapes at low and high temperatures derives from the interplay of diffusion-mediated aggregation with different aspects of a corner diffusion anisotropy. The broken symmetry is less clear at intermediate temperatures, where the near-isotropic fractal shapes reflect in part a kink Ehrlich-Schwoebel effect.

DOI: 10.1103/PhysRevB.71.115414 PACS number(s): 68.55.Jk, 68.55.Ac, 68.37.Ef, 81.15.Aa

I. INTRODUCTION

Ag/Ag(111) provides a classic example of a homoepitaxial growth system where multilayer growth exhibits rapid kinetic roughening and the formation of "wedding cakes," i.e., multilayer stacks of two-dimensional islands.[1–3] Both features are associated with a large Ehrlich-Schwoebel (ES) step-edge barrier inhibiting downward interlayer transport, although its magnitude for Ag/Ag(111) is still uncertain.[4–7] These features are regarded as characteristic of other metal(111) homoepitaxial systems, as is "reentrant smooth growth" at lower temperatures. The latter has been associated with development of irregular islands having lower effective ES barriers.[8–10]

Somewhat surprisingly, there has been no comprehensive real-space characterization of the temperature dependence of either submonolayer island formation or multilayer growth morphologies in this system. Some earlier studies focused on room temperature behavior, where the characteristic lateral length scale is so large that the morphology is influenced by defects (dislocations) in the substrate.[1] Thus, the primary goal of this contribution is to provide a systematic study of the dependence of submonolayer island growth shapes on deposition temperature (T). This knowledge is a prerequisite to detailed analysis and modeling of multilayer growth. Indeed, it is well recognized that for systems with large ES barriers, submonolayer islands form the bases of multilayer mounds. Thus, island structure strongly impacts multilayer morphologies.[11]

For metal(111) systems, straight low-energy steps at island edges with orientations differing by 60° alternate between so-called *A*- and *B*-type steps. These differ in the local atomic geometry, as will be illustrated explicitly below. A convenient feature of the Ag/Ag(111) system as regards island morphologies is that energies of *A*- and *B*-type steps are almost identical.[12–14] Thus, the equilibrium island shape is almost perfectly hexagonal, and any deviations from this shape or reduction from sixfold to threefold symmetry reflect kinetic effects related to growth. In contrast, other well-studied systems such as Pt/Pt(111) and Al/Al(111) display clear reductions from sixfold to threefold symmetry, e.g., compact triangular island growth shapes, due in large part to a difference in *A*- and *B*-step-edge energies.[11]

For low-T epitaxial growth on fcc(111) and hcp(0001) surfaces, one often observes fractal or dendritic islands.[15] Here, the term fractal refers to the case where the irregular structure is isotropic, and dendritic implies some overall symmetry related to that of the underlying substrate. These irregular shapes derive from restricted periphery diffusion (PD) of adatoms at the island edges. Specifically, PD-mediated island shape relaxation is not efficient enough to quench the instability in island shapes which arises as a natural consequence of terrace-diffusion-mediated island growth. This instability is often referred to as the Mullins-Sekerka instability[16] in the context of continuum models of interface propagation, or as the diffusion-limited-aggregation (DLA) instability in the context of atomistic models where aggregating atoms stick at the impact sites.[17]

Island growth structure in metal(111) homoepitaxy invariably differs from simple DLA models.[17] This is because even at the lowest T studied, adatoms at the island edges can typically move locally from singly to higher coordinated sites in these systems,[18] and for most T some longer-range PD is operative. Actually, for moderate T, even the simplest "tailored model" with a single PD rate for all edge atoms not trapped at kink sites does a reasonable job of describing experimental observations made in several systems of fractal islands with "fat" arms.[19]

In addition, more detailed modeling has been performed for various specific systems by including numerous PD bar-

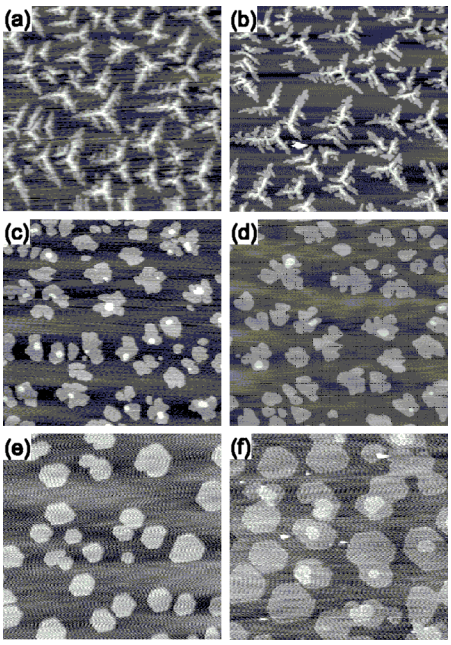

FIG. 1. STM images of island distributions formed after deposition of 0.3 ML Ag on Ag(111) with a deposition rate of 3.5×10^{-3} ML/s at different temperatures: (a) 120, (b) 135, (c) 150, (d) 165, (e) 180, and (f) 200 K. Each image size is 300×300 nm^2.

riers obtained from electronic structure calculations.[20] Of particular importance for this study is a "corner diffusion anisotropy" phenomenon discovered in these previous studies.[21,22] This phenomenon reflects the feature that adatoms which are singly coordinated or singly bonded to other adatoms at the island edge can more easily undergo edge diffusion "around the corner" in one direction (where the diffusion path is through a bridge site) than in the opposite direction (through an on-top site). One consequence for low-T growth is that terrace adatoms which aggregate by forming a single bond with isolated adatoms along step edges can less readily relax to higher-coordinated sites at A steps than at B steps. Thus, outward growth at A steps is more rapid, resulting in dendrites with triangular envelopes having sides aligned along the direction of B steps. This low-T growth phenomenon has been analyzed in detail for Ag/Pt(111) by Brune *et al.*,[21] for Pt/Pt(111) by Hohage *et al.*,[22] and for Al/Al(111) by Ovesson *et al.*[23] It is also expected to occur in other metal(111) systems, such as Ag/Ag(111).

In Sec. II, we briefly describe our experimental procedures, and then in Sec. III present our observations on island structure utilizing variable-temperature scanning tunneling microscopy (VTSTM). In Sec. IV, we present the atomistic lattice-gas model for island growth. Extensive comparison between experiments and modeling is also provided in Secs. III and IV. Next, in Sec. V we discuss in more detail the atomistic mechanisms underlying the observed growth. Finally, our conclusions are presented in Sec. VI.

II. EXPERIMENTAL DETAILS

The Ag sample used in these studies was prepared by Princeton Scientific using a chemical etching process and was oriented to the (111) direction. Subsequent polishing (after sample degradation) was performed at Ames Laboratory using 6, 1, and 0.25 μm diamond pastes, with a final polish using 0.025 μm colloidal silica.

All experiments were carried out in ultrahigh vacuum (UHV) with a typical base pressure $\sim 1 \times 10^{-10}$ Torr. Thin film deposition of Ag on the Ag(111) single-crystal surface between 120 and 200 K was performed using an Omicron EFM3 UHV evaporator containing Ag (99.994% pure) as the deposition source. The flux was held fixed at $F = 0.003$–0.004 monolayers (Ml)/s in all experiments. Film morphology was examined using an Omicron variable-temperature scanning tunneling microscope. Large flat terraces were observed, sometimes up to 0.5 μm in width. The height of monatomic steps bordering these terraces was consistent with the known value of 0.235 nm for Ag.

Cooling of the sample was achieved using liquid nitrogen. Temperature measurements for the sample were taken by means of a silicon diode at the coupling stage. The accuracy of the sensor (Lakeshore Temperature Controller) is ±1 K below 100 K (±1% above 100 K). The temperature difference between the coupling stage and the sample depends on the absolute temperature and the sample mounting. As a guideline, when $T_{diode} \sim 100$ K, the offset is roughly 15 K, and $T_{sample} = T_{diode} + \text{offset}$, with a reliability of ±5 K. We have used this type of adjustment to determine sample temperatures, and henceforth only these will be reported.

III. EXPERIMENTAL OBSERVATIONS ON ISLAND SHAPES

Below, we describe in detail our observations on the growth shapes of Ag islands formed by deposition on Ag(111) at different temperatures. To facilitate the comparison of experiment and modeling, we present STM images of island shapes together with those from simulations of our atomistic model. The details of this model and the associated parameter choices will be described in subsequent sections. We should note that the STM images typically show second-layer population (the lightest regions). This is associated with atoms depositing on top of islands where they likely remain due to the large ES barrier and nucleate second-layer islands. The same phenomenon occurs in our simulation model (where there is no interlayer transport), but the second-layer islands are not shown in the simulation images. In addition, in this section, we provide some comments on previous experimental observations for this system.

Figure 1 presents experimental island shapes for deposition at 120, 135, 150, 165, 180, and 200 K, and Fig. 2 shows the corresponding kinetic Monte Carlo (KMC) simulation results. Island shape transitions with increasing temperature can be clearly observed. At low T (120 and 135 K), dendritic islands with triangular envelopes are visible and characterized by preferential branch growth in the $\langle \overline{112} \rangle$ directions, i.e., perpendicular to A steps. At intermediate T (150 and 165 K), islands are more compact than those at low T, but still exhibit some degree of fractal shape instability with thicker arms, and with fairly isotropic overall structure. At high T (180 and 200 K), islands with somewhat distorted

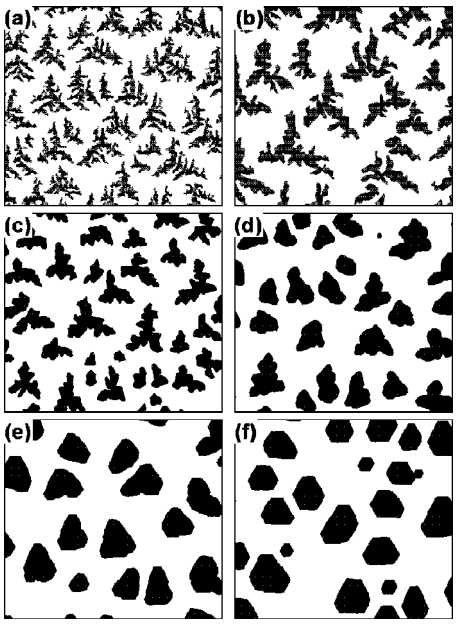

FIG. 2. Island shapes obtained from KMC simulations of a realistic atomistic model after deposition of 0.3 ML with a rate of 3.55×10^{-3} ML/s at temperatures of (a) 120, (b) 135, (c) 150, (d) 165, (e) 180, and (f) 200 K. The image sizes are 135×135 nm^2 in (a),(b), and 202×202 nm^2 in others.

hexagonal shapes are observed. There is generally good agreement between experiment and simulations.

Dendritic shapes of Ag/Ag(111) islands formed by deposition at low $T\approx110$ K were also reported in one previous experimental study,[21] consistent with our observations. No detailed analysis was performed of this previous image. However, it was argued that the corner diffusion anisotropy experienced by aggregating adatoms plays the key role in the formation of the triangular envelope of the dendrites.[21] Our modeling supports this claim, as discussed in more detail in Sec. V.

One other image of an irregular fractal-like island formed by deposition at 150 K has been reported previously.[24] The arms in that island were somewhat more prominent than in our 150 K STM images, but similar to our simulated shapes. Indeed, it is possible that the temperature for our STM image is slightly above 150 K, and that for the previous image is slightly below 150 K, explaining the apparent discrepancy. The focus of this previous study was on assessing the thickening of the fractal arms due to enhanced edge diffusion with increasing T within the framework of a model with a single PD barrier.[19] Our more detailed studies in Sec. V demonstrate the key role that inhibited kink rounding plays relative to edge diffusion, thus requiring a more complex modeling and analysis than suggested in that previous work.

There seem to be no previous growth studies of the specific higher-T regime where edge diffusion and kink rounding become sufficiently facile to produce a transition to compact distorted hexagonal shapes. Thus, our observation that this transition occurs at around 180 K provides particularly valuable input for modeling. One unexpected observation is that even at 190 or 200 K where islands are large and compact, there is still significant breaking of sixfold symmetry in

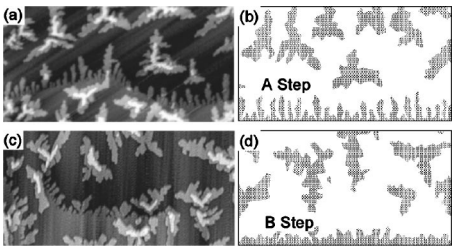

FIG. 3. STM images comparing growth of extended *A*-type (a) and *B*-type (c) steps at 135 K. Corresponding KMC simulation images are shown in (b) and (d). The image sizes are 230×100 nm^2 in (a), 144×84 nm^2 in (c), and 138×68 nm^2 in (b)and (d).

both experiment and simulation. Specifically, islands are distorted hexagons with longer *B* steps than *A* steps. This could be a consequence of a corner diffusion anisotropy (although the density of corners is quite low at high T), or perhaps due to other kinetic anisotropies. We explore this issue further in Sec. V.

Next, rather than discussing shapes of individual islands, we explore related phenomena including growth at extended step edges, and the interference effect on island growth of nearby islands and ascending steps. In Fig. 3, we show STM images and corresponding simulations at 135 K of growth due to aggregation at ascending extended *A*- and *B*-type step edges on Ag(111). Similar to the growth behavior observed in the Pt/Pt(111) system,[22] while the *A* step grows very rough, the *B* step remains relatively smooth. The behavior is consistent with and expected from our observations of growth of individual islands: *A* steps tend to grow out in favor of *B* steps.

Finally, in our experiments, the influence of the diffusion field on island growth is dramatic. Figure 4(a) shows that growth of nearby islands is greatly distorted during deposition of 0.3 ML Ag at 135 K. The islands labeled by 1 and 2 have nucleated quite close together, and apparently almost simultaneously (given their roughly equal size). The growth of their tips pointing toward each other is strongly screened due to interaction of their diffusion fields. Similar situations arise in kinetic Monte Carlo simulations as shown in Fig. 4(b). For islands growing nearby ascending extended steps, there is no strong perturbation on shape despite the significant influence of the step on the diffusion field.

IV. ATOMISTIC LATTICE-GAS MODEL FOR ISLAND GROWTH

In this section, we describe the details of our atomistic lattice-gas modeling of island nucleation and growth during deposition for metal(111) homoepitaxial systems. Below, *c*, *e*, and *k* will denote one-, two-, and three-coordinated corner, edge, and kink sites, respectively, where $e=A$- or *B*-type steps. See Fig. 5, which also illustrates the distinct structure of *A*- and *B*-type steps. First, we describe in some detail those features of the modeling which pertain to growth of an individual island.

(i) Adatoms reside only at fcc sites, and hop directly between such sites, although rates or barriers reflect the diffu-

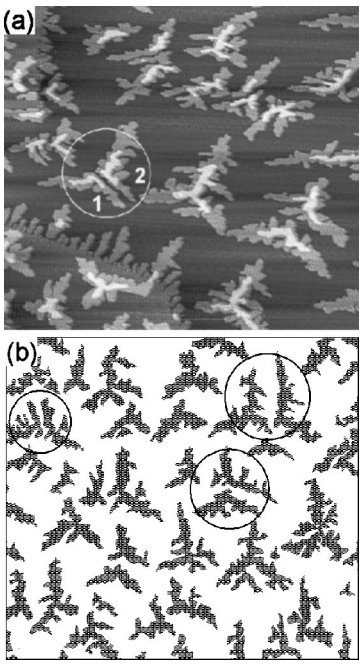

FIG. 4. Illustration of the influence of the diffusion field on the growth of nearby pairs of islands at 135 K. (a) STM image, (b) KMC simulation. Each image size is 202×202 nm^2.

sion pathway, e.g., through intervening hcp sites. As an aside, we note that only a small fraction of hcp or "stacking fault" islands are observed in our experimental studies (relative to the population of fcc islands). This feature will be discussed in more detail elsewhere.

(ii) Deposited atoms diffuse across the surface and aggregate irreversibly with the edge of a nearby island. (Islands effectively just accumulate adatoms that land within "capture zones" surrounding them.[25]) Detachment or evaporation from island edges is not significant for temperatures considered here. The effective barrier for evaporation is given by the barrier for detachment from kinks.[26] The embedded-atom method (EAM) value of 0.76 eV for this barrier is consistent

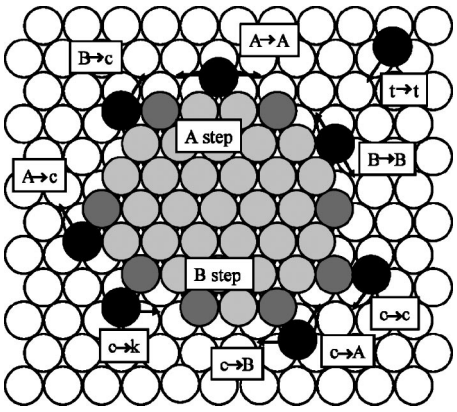

FIG. 5. Illustration of the *A*- and *B*-type steps on fcc(111) surfaces, and the elementary diffusion processes. *t*, *c*, *e*, and *k* denote terrace, corner, edge, and kink sites, respectively. The white, gray, and black circles denote the substrate, island, and mobile atoms, respectively. The balls colored dark gray are corners of the island.

TABLE I. Values for key PD barriers in meV (rounded to the nearest 5 meV), where KMC indicates values chosen in our modeling. In addition, the EAM predicts that $E_{A\to c\to k}=380$ meV and $E_{B\to c\to k}=380$ meV (which are both set to 360 meV in KMC). EMT indicates the effective medium theory.

	$E_{A\to A}$	$E_{B\to B}$	$E_{c\to A}$	$E_{c\to B}$	$E_{e\to c\to e}$
EMT (Ref. 21)	220	300	75	140	330
EAM	295	340	75	150	390
KMC	275	310	75	150	360

with observed rates for Ostwald ripening.[27] The corresponding detachment rate is negligible compared with the aggregation rate.

(iii) Step-edge atoms undergo PD hopping between one-, two-, and three-coordinated sites. Triply coordinated kink sites effectively act as irreversible trap sites for the time scale and temperatures of relevance in our study. This follows since the EAM barriers for escape from kinks to step edges are $E_{k\to A}=0.47$ eV and $E_{k\to B}=0.54$ eV. These are significantly higher than the PD barriers included in Table I. The corresponding escape rates of $\sim 10^{-4}$/s at 150 K, and $\sim 10^{0.4}$/s at 200 K are far below the aggregation rate, so kink escape is not significant. Thus, the islands generated by the model have nonequilibrium growth shapes, since true equilibration requires escape from kinks.

(iv) The key model parameters are PD barriers describing edge diffusion $e\to e$, corner to edge hopping $c\to e$, kink rounding $e\to c\to k$, and corner rounding $e\to c\to e$ (for $e=A$ and B). Effective barriers are determined by the highest energy on the overall diffusion path relative to the initial energy, so corner rounding in either direction, $A\to c\to B$ and $B\to c\to A$, has the same effective barrier. See the Appendix and Fig. 6(a). To reduce the number of parameters in our modeling, we set the three effective barriers for kink and corner rounding ($A\to c\to k$, $B\to c\to k$, and $e\to c\to e$) to be equal. Other constraints are imposed by equality of *A*- and *B*-step energies, and by detailed balance. We choose a common prefactor for all PD processes of $\upsilon=10^{13}$/s.

Selected values for barriers shown in Fig. 6 are guided at least in part by a previous effective medium theory (EMT) study,[21] and by our own more extensive embedded-atom method studies. Table I compares our chosen barriers for KMC simulation with those predicted by the EAM and EMT. Note that values quoted for corner and kink rounding are for a conventional single-atom-hopping mechanism. We have checked with the EAM that barriers associated with a two-atom exchange process are higher by about 0.2 eV for the Ag/Ag(111) system.

Note that the corner diffusion anisotropy, mentioned above, is reflected in the different values for $E_{c\to A}=0.075$ eV and $E_{c\to B}=0.15$ eV. See Fig. 6(a). This anisotropy is felt by adatoms which aggregate at the corners of distorted hexagonal islands at higher *T*, and influences the associated growth shapes. See Sec. V for further discussion. Furthermore, we note that corner diffusion anisotropy is also operative in so-called corner to kink $c\to k$ hopping where it is harder to reach kinks at *A* steps [Fig. 6(b)] than those at *B*

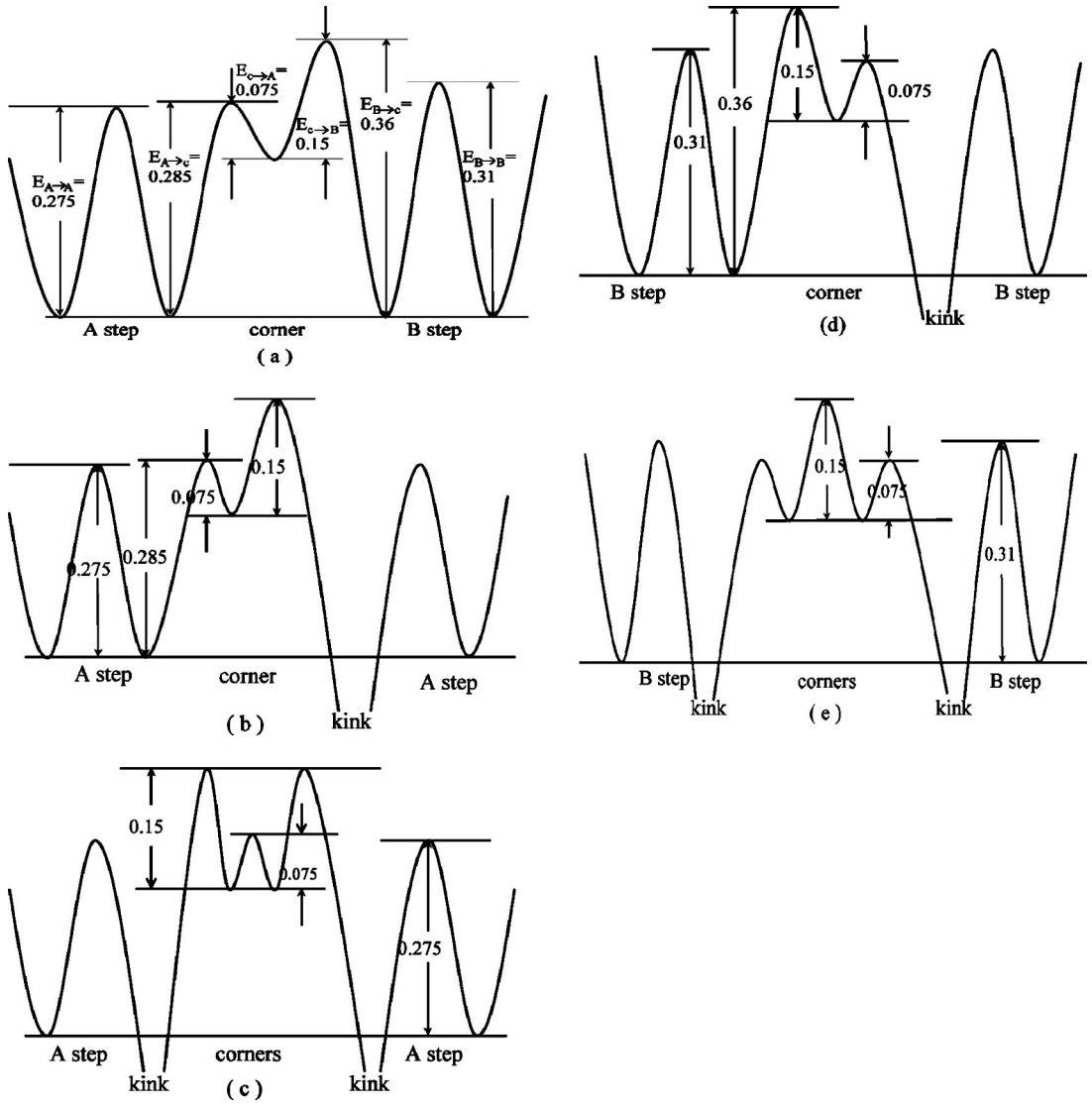

FIG. 6. Potential energy surface for periphery diffusion associated with corner rounding between *A* and *B* steps (a); kink rounding on an *A* (b) and a *B* step (d); relaxation to a kink site of an atom singly coordinated to another isolated atom on an *A* (c) and a *B* step (e). The unit of energy barriers is eV.

steps [Fig. 6(d)]. Of particular significance for low-*T* growth is the situation where an aggregating atom attaches to a single atom on a straight step edge. One such configuration is illustrated in the far right side of Fig. 5. Here, the barrier to relax to the kink site is chosen as 0.15 eV for the *A* step [Fig. 6(c)] and 0.075 eV for the *B* step [Fig. 6(e)]. This feature produces dendrites with a triangular envelope at low *T* as noted above and in previous work,[21,22] and discussed further in Sec. V. Finally, we remark that the same relaxation anisotropy will be operative when aggregating atoms attach to sites at the corners of strings of atoms at *A*- and *B*-step edges (which are typically short at low *T*).

As an aside, we note that for the most part singly coordinated corner adatoms can hop essentially instantaneously to higher-coordinated sites, since there is usually a pathway to reach such doubly or triply coordinated sites with a barrier of only 0.075 eV. However, one exception is where a single-atom-thick finger of sites develops, and the atom attached at the corner has a higher barrier of 0.15 eV to hop in either direction to reach an *A* step. See Fig. 6(c). Then, the singly coordinated atom is temporarily trapped making rapid $c \rightarrow c$ hops with low barrier of 0.075 meV as shown in the far right side of Fig. 5. These configurations are not uncommon for the lowest *T* of interest here.

Given the sensitivity of island shapes to certain key barriers, and given the limitations in accuracy of semiempirical (and even *ab initio*) methods, our ultimate choice of parameters is primarily driven by the requirement of agreement with experiment. Specifically, optimization of the choice of barriers in our KMC modeling was achieved through a three stage process. First, we focused on adjusting the anisotropy in the corner to edge (or kink) barriers in order to recover the dendritic island shapes at low *T*. Then, we adjusted the edge diffusion barriers in order to obtain appropriate thickening of fractal arms of islands upon increasing *T*. Finally, we adjusted the edge to corner barriers (and thus the effective barrier for kink or corner rounding) to achieve a transition to compactification around 180 K. Of course, there is some un-

certainty in the values of these parameters. For example, by slightly decreasing edge diffusion and kink rounding barriers, simulated island shapes at 150 K would become somewhat more regular, certainly consistent with our data (but less like those in Ref. 24).

Next, we discuss the additional features incorporated into our simulations for nucleation and growth of multiple islands. The key factor controlling island structure is the relative magnitude of rates for PD and for aggregation of single atoms with islands. See Sec. V. The latter is given by F/N_{isl} where $F=0.0035$ ML/s is the deposition flux, and N_{isl} is the island density (per site). Thus, one can reasonably assess island structure using simulations of growth of a single island in a system of size selected to give the correct N_{isl} (and using the experimental F). However, in deposition processes, islands are not periodically distributed, and shapes of individual islands are strongly affected by the positions of surrounding islands due to diffusion field effects. Thus, to capture this feature, we perform simulations of nucleation and growth of many islands during deposition, where we fine-tune terrace diffusion parameters to recover the experimentally observed island density for each temperature of interest. These densities (per fcc site) vary from $\sim 1\times 10^{-4}$ at 120–135 K, to $\sim 5\times 10^{-5}$ at 150–165 K, to $\sim 2\times 10^{-5}$ at 180–200 K. See the Appendix for further discussion.

There is one feature of the Ag/Ag(111) deposition process which allows for a convenient simplification in our modeling. There is little contribution to island growth from atoms landing on top of islands at the submonolayer coverages and temperatures considered here.[2,10] This is expected due to the presence of a large Ehrlich-Schwoebel barrier, and due to the low T considered here. Consequently, this contribution is neglected in our modeling. Our analysis of populations of different layers, in more extensive studies focused on multilayer growth, supports this claim.[10]

The KMC simulations of the atomistic lattice-gas model were performed on a large ($\sim 10^6$ site) six-coordinated triangular lattice representing the fcc sites on a fcc(111) surface. Periodic boundary conditions were imposed. A Bortz-type algorithm[11] was used which tracked different classes of diffusing terrace and step-edge adatoms.

V. DISCUSSION AND ADDITIONAL MODELING ANALYSIS

A. Basic analysis of island shape stability

Formation of compact or regular island shapes requires that adatoms aggregating at the island edge have enough time to reach kink sites between aggregation events, thus avoiding capture by other aggregating atoms to form new outer rows. Thus, it is natural to compare the characteristic time between aggregation events, $\tau_{agg}\sim N_{isl}/F$, with the characteristic time τ_{PD} to reach a kink via periphery diffusion for a typical kink-free step-edge length of L. Here L is measured in lattice constants, N_{isl} is the island density per fcc site, and $F=0.0035$ ML/s is the deposition flux. If τ_{PD} is controlled by diffusion along straight steps, then $\tau_{PD}(e\to e)\sim L^2/(12h_{e\to e})$.[11,19] If it is controlled by kink rounding, then $\tau_{PD}(e\to c\to k)\sim L/(2h_{e\to c\to k})$, where the factor of L reflects a probability of $1/L$ for the edge atom to be adjacent to the kink. Here, h denotes hop rates (per second) for PD processes.[28,29] In general, one has $\tau_{PD}=\tau_{PD}(e\to e)+\tau_{PD}(e\to c\to k)$. In Table II, we compare values of these characteristic times at various T using parameters appropriate for the Ag/Ag(111) system. One can see that shape instability is driven predominantly by limited kink rounding, and should occur at 135 and 165 K for expected values of $L\sim 10$ (where $\tau_{agg}<\tau_{PD}$) or above, but not at 200 K for $L\sim 50$ (where $\tau_{agg}>\tau_{PD}$).

TABLE II. Comparison of characteristic times for aggregation, τ_{agg}, and for transport to kinks, τ_{PD}.

T(K)	τ_{agg}(s)	$\tau_{PD}(B\to B)$(s)	$\tau_{PD}(e\to c\to k)$(s)
135	$10^{-1.5}$	$L^2\times 10^{-2.5}$	$L\times 10^{0.1}$
165	$10^{-2.0}$	$L^2\times 10^{-4.6}$	$L\times 10^{-2.3}$
200	$10^{-2.2}$	$L^2\times 10^{-6.3}$	$L\times 10^{-4.2}$

B. Analysis of the effect of corner diffusion anisotropy

As noted above and in previous studies,[21,22] one manifestation of this anisotropy is to produce dendritic islands at low T. Specifically, aggregating adatoms attaching to single adatoms or the corners of short strings of adatoms at step edges can more readily relax to kink sites at B steps than at A steps. Compare Fig. 6(e) with Fig. 6(c). As described in Sec. IV, this leads to faster growth orthogonal to A steps.

For high enough T, islands become distorted hexagons bordered by fairly straight A- and B-step edges having a quite low density of corner and kink sites at their edges. Thus, one might expect the effect of the anisotropy to become insignificant. However, our experimental observations and simulations suggest that even around 200 K, the weakened anisotropy still affects island shape. In this regime, the anisotropy can exert its influence in the following way. Adatoms diffusing across a terrace to a corner site separating A- and B-step edges of an island tend to subsequently hop to the A step more often than to the B step due to an asymmetry in the potential energy surface for PD at the corner. The effect of corner diffusion anisotropy is to cause A steps to propagate faster than B steps, thus causing the A steps to disappear or "grow out," leaving islands with predominantly B steps. We should caution that anisotropy in edge diffusion could also produce distorted hexagons at higher T, although this does not seem to be the case for the Ag/Ag(111) system (see below).

In order to unambiguously assess this affect of corner diffusion anisotropy, we performed additional simulations without anisotropy of corner rounding aggregation at 120 and 200 K, respectively. Clearly, at low T (120 K), removal of the anisotropy produces isotropic fractal shapes. Compare Figs. 7(a) and 7(b). At high T (200 K), removal of the anisotropy produces on average near-hexagonal islands, in contrast to the preference for longer B steps with the anisotropy. Compare Figs. 7(c) and 7(d).

C. Analysis of island shapes at moderate T: Kink Ehrlich-Schwoebel effect

At moderate T of 150 or 165 K, it seems that any breaking of sixfold symmetry is somewhat hidden by the irregular

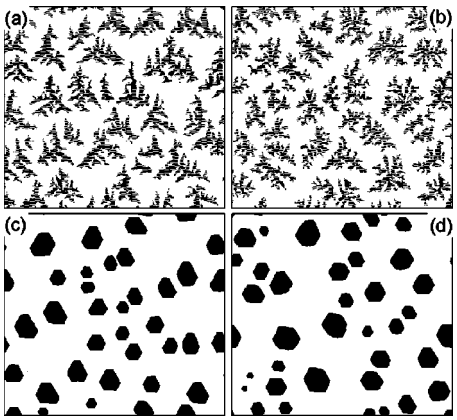

FIG. 7. Demonstration of effect of the corner diffusion anisotropy on island growth shapes for 0.3 ML deposition. Simulations with (a) and without (b) this anisotropy at 120 K. Corresponding results for 200 K are shown in (c) and (d). The system size is 202×202 nm^2.

island shapes. It is appropriate to ask, what is the main factor producing the shape instability at these temperatures? The simple analysis in Sec. V A above suggests that limited kink rounding[30] may be more significant than limited edge diffusion. To test this assertion, we have performed simulations with a reduced kink (or corner) rounding barrier to compare against those with our previously selected barriers. Indeed, we find that as the kink rounding barrier is reduced, the islands become significantly more compact, and in fact adopt strongly symmetry-broken distorted triangular shapes. See Fig. 8.

D. Symmetry breaking and mass transport between step edges

The broken sixfold symmetry clearly can result from corner diffusion anisotropy, but it can also derive from edge diffusion anisotropies.[31,32] Subtleties with regard to the latter have caused some confusion even in the simplest case of equal *A*- and *B*-step energies. Initially, it was argued that slower edge diffusion along *B* steps would lead to rougher, more rapidly advancing *B* steps, causing *B* step edges to grow out. In fact, as discussed in Ref. 11, the opposite is true. Slower *B* edge atoms are less efficiently captured by kinks (despite the enhanced kink density), so the population of adatoms on the *B* edge is higher than on the *A* edge. This

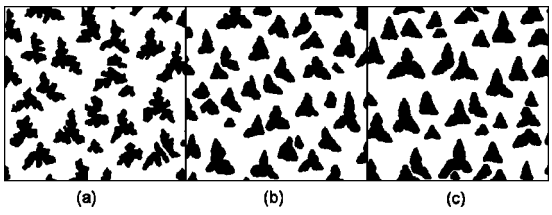

FIG. 8. Illustration of kink Ehrlich-Schwoebel effect on island growth shapes for 0.3 ML deposition at $T=150$ K. (a) $E_{A\to c}=0.285$ eV, $E_{B\to c}=0.36$ eV; (b) $E_{A\to c}=0.275$ eV, $E_{B\to c}=0.33$ eV; (c) $E_{A\to c}=0.275$ eV, $E_{B\to c}=0.31$ eV. In all cases, $E_{A\to A}=0.275$ eV and $E_{B\to B}=0.31$ eV. The image size is 81×81 nm^2.

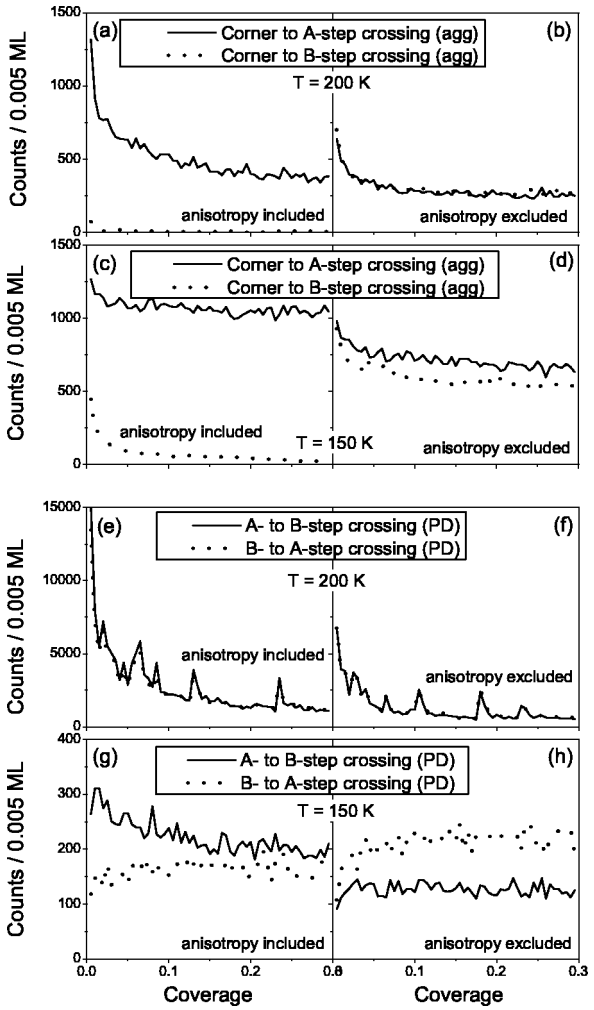

FIG. 9. Simulation results at 200 K for corner to edge fluxes of aggregating adatoms with (a) and without (b) corner diffusion anisotropy. Corresponding results are shown in (c) and (d) for 150 K. Simulation results at 200 K for *A*- to *B*-step-edge PD fluxes, and *B*- to *A*-step-edge fluxes with (e) and without (f) corner aggregation anisotropy. Corresponding results are shown in (g) and (h) for 150 K. The system size in simulation is 270×270 nm^2.

leads to a net mass flow from *B* to *A* edges, which causes *A* edges to grow out. Hence, this edge diffusion anisotropy would act in the same direction as corner aggregation anisotropy for the Ag/Ag(111) system.

One way to quantify these phenomena is to augment simulations to monitor the relative fluxes of atoms which have aggregated at corner sites separating straight *A* and *B* steps and then hop to the *A*-versus *B*-step edges. For such adatoms, we compare the flux going to *A* steps with that to *B* steps at 200 K in Fig. 9(a) and at 150 K in Fig. 9(c). As expected, with corner diffusion anisotropy, the former flux is far higher. In refined simulations without this anisotropy, the two fluxes become almost equal. See Figs. 9(b) and 9(d).

In addition, we examine the PD flux between *A*- and *B*-step edges at 200 K in Fig. 9(e) and at 150 K in Fig. 9(g). One finds that these fluxes roughly balance at 200 K with or without corner diffusion anisotropy. See Figs. 9(e) and 9(f). However, at 150 K, the presence of corner diffusion aniso-

tropy significantly enhances the population of adatoms on *A* steps relative to *B* steps. Thus, one expects a net flow of adatoms from *A* to *B* steps to counter this imbalance as confirmed in Fig. 9(g). The *A*-step edges still grow out since the effect shown in Fig. 9(c) still dominates. If one removes this corner diffusion anisotropy (but maintains the edge diffusion anisotropy), then one finds a net mass flow from *B* to *A* steps. This is due to the edge diffusion anisotropy, for reasons described above. See Fig. 9(h). However, the magnitude of this net flux is fairly small, and it does not have much effect on island shapes. As already indicated in Sec. V B, while the edge diffusion anisotropy is operative in this system, it has a relatively minor effect on island shapes compared to corner diffusion anisotropy.

VI. CONCLUSIONS

We have systematically studied the temperature dependence of island growth shapes in submonolayer deposition of Ag on Ag(111) surface between 120 and 200 K. Island shapes progress from dendrites with triangular envelopes at low *T* to more isotropic fractals at intermediate *T*, and then to distorted hexagons at high *T*. Since energies for *A* and *B* steps are almost identical, observed reduction from sixfold to threefold symmetry must reflect kinetic anisotropies. KMC simulations of a realistic atomistic model provide detailed insight into the underlying microscopic mechanics. The choice of activation barriers for PD in the modeling is guided by EMT and EAM calculations, but fine-tuned to match experimental observations. Corner diffusion anisotropy has a strong influence on shapes at both high and low *T*. The effect of small additional barriers for kink rounding is significant at moderate *T*. Our successful development of a predictive atomistic model for submonolayer island shapes is a necessary precursor to our planned development of a realistic multilayer growth model.[10]

ACKNOWLEDGMENTS

M.L. thanks Dr. Da-Jiang Liu for helpful discussions. E.C., M.L., P.W.C., C.G., C.J.J., J.W.E., and P.A.T. were supported for this work by NSF Grant No. CHE-0414378. It was performed at Ames Laboratory, which is operated for the U.S. Department of Energy by Iowa State University under Contract No. W-7405-Eng-82. T.S.R. was supported by NSF Grant No. EEC-0085604.

APPENDIX: FURTHER DETAILS OF ISLAND NUCLEATION AND GROWTH

Below, we comment further on two specific issues related to island formation.

(i) The effective rate for corner rounding from a straight *B*-step edge to a straight *A*-step edge $h_{B\to c\to A}$ is controlled by the slow rate $h_{B\to c}\sim \nu \exp(-0.36\ \mathrm{eV}/k_BT)$ to reach the corner. Here k_B is the Boltzmann constant. The rate for *A*- to *B*-step corner rounding is $h_{A\to c\to B}=h_{c\to B}\rho_c$, where ρ_c is the population of corner (relative to edge) sites. Here $h_{c\to B}\sim\exp(-0.15\ \mathrm{eV}/k_BT)$ and $\rho_c\sim\exp(-\delta E/k_BT)$ where $\delta E=0.21$ eV is the difference between corner and edge energy. Thus, effective corner rounding rates in both directions are identical, as stated in Sec. IV. This is a consequence of the equality of *A*- and *B*-step energies.

(ii) Our observed island densities for coverage $\sim$0.3 ML and 120–200 K are reasonably consistent with results from Brune *et al.*[33] at 50–130 K. The latter, which are for much lower coverage and lower flux, are fit by simulations for irreversible island formation with terrace diffusion barrier $E_d=0.10$ eV and $\nu=10^{11}$/s. The "low" value of ν likely reflects some influence of longer-range repulsive interactions.[11,34] Early experiments suggested that some type of transition occurs at about 130 K.[35] If this is the onset of reversible island formation, standard analysis implies an adatom pair bond energy of $\sim$0.15 eV,[36] which is quite plausible although significantly lower than a recent *ab initio* estimate.[34] However, one should also consider other scenarios, e.g., dimer mobility.

*Corresponding author. Email address: maozhi@scl.ameslab.gov

[1] J. Vrijmoeth, H. A. Van der Vegt, J A. Meyer, E. Vlieg, and R. J. Behm, Phys. Rev. Lett. **72**, 3843 (1994).
[2] E. Z. Luo, J. Wollschläger, F. Wegner, and M. Henzler, Appl. Phys. A: Mater. Sci. Process. **60**, 19 (1995).
[3] W. C. Elliott, P. F. Miceli, T. Tse, and P. W. Stephens, Phys. Rev. B **54**, 17 938 (1996).
[4] K. R. Roos and M. C. Tringides, Phys. Rev. Lett. **85**, 1480 (2000); **87**, 149602 (2001); **87**, 149604 (2001); **87**, 149606 (2001).
[5] J. Krug, Phys. Rev. Lett. **87**, 149601 (2001).
[6] K. Morgenstern and F. Besenbacher, Phys. Rev. Lett. **87**, 149603 (2001).
[7] S. Heinrichs and Ph. Maass, Phys. Rev. Lett. **87**, 149605 (2001).
[8] R. Kunkel, B. Poelsema, L. K. Verheij, and G. Comsa, Phys. Rev. Lett. **65**, 733 (1990).
[9] M. Henzler, T. Schmidt, and E. Z. Luo, *Structure of Surfaces* (World Scientific, Singapore, 1994), Vol. IV.
[10] Maozhi Li *et al.* (unpublished).
[11] T. Michely and J. Krug, *Islands, Mounds and Atoms: Patterns and Processes in Crystal Growth Far from Equilibrium* (Springer, Berlin, 2004).
[12] M. Giesen, Prog. Surf. Sci. **68**, 1 (2001).
[13] K. Morgenstern, G. Rosenfeld, E. Lagsgaard, F. Besenbacher, and G. Comsa, Phys. Rev. Lett. **80**, 556 (1998).
[14] M. Giesen, C. Steimer, and H. Ibach, Surf. Sci. **471**, 80 (2001).
[15] R. Q. Hwang and M. C. Bartelt, Chem. Rev. (Washington, D.C.) **97**, 1063 (1997).
[16] W. W. Mullins and R. F. Sekerka, J. Appl. Phys. **35**, 444 (1964).
[17] T. A. Witten and L. M. Sander, Phys. Rev. Lett. **47**, 1400 (1981).
[18] Z. Zhang, X. Chen, and M. G. Lagally, Phys. Rev. Lett. **73**, 1829 (1994).

[19] M. C. Bartelt and J. W. Evans, Surf. Sci. **314**, L829 (1994).
[20] A. Bogicevic, J. Strömquist, and B. I. Lundqvist, Phys. Rev. Lett. **81**, 637 (1998).
[21] H. Brune, H. Röder, K. Bromann, K. Kern, J. Jacobsen, P. Stoltze, K. Jacobsen, and J. Norskov, Surf. Sci. **349**, L115 (1996).
[22] M. Hohage, M. Bott, M. Morgenstern, Z. Zhang, T. Michely, and G. Comsa, Phys. Rev. Lett. **76**, 2366 (1996).
[23] S. Ovesson, A. Bogicevic, and B. I. Lundqvist, Phys. Rev. Lett. **83**, 2608 (1999).
[24] H. Röder, K. Bromann, H. Brune, and K. Kern, Phys. Rev. Lett. **74**, 3217 (1995).
[25] M. C. Bartelt, C. R. Stoldt, C. J. Jenks, P. A. Thiel, and J. W. Evans, Phys. Rev. B **59**, 3125 (1999).
[26] Lower barriers for detachment of edge or corner atoms are offset by the lower populations of such atoms.
[27] K. Morgenstern, G. Rosenfeld, and G. Comsa, Phys. Rev. Lett. **76**, 2113 (1996).
[28] J. Zhong, T. Zhang, Z. Zhang, and M. G. Lagally, Phys. Rev. B **63**, 113403 (2001).
[29] K. J. Caspersen and J. W. Evans, in *Atomistic Aspects of Epitaxial Growth*, edited by M. Kotrla *et al.*, NATO Advanced Research Workshop Series II: Mathematics, Physics and Chemistry, Volume 65 (Kluwer, Dordrecht, 2002), p. 197.
[30] O. Pierre-Louis, M. R. D'Orsogna, and T. L. Einstein, Phys. Rev. Lett. **82**, 3661 (1999).
[31] J. Jacobsen, K. W. Jacobsen, and J. K. Norskov, Surf. Sci. **359**, 37 (1996).
[32] H. Johnsson, Annu. Rev. Phys. Chem. **51**, 623 (2000).
[33] H. Brune, K. Broman, and K. Kern, in *Surface Diffusion: Atomistic and Collective Processes*, edited by M. Tringides, NATO Advanced Studies Institute, Series B: Physics (Plenum, New York, 1997), Vol. 360, p. 135.
[34] K. A. Fichthorn and M. Scheffler, Phys. Rev. Lett. **84**, 5371 (2000).
[35] G. Rosenfeld, N. N. Lipkin, W. Wulfhekel, J. Kliewer, K. Morgenstern, B. Poelsema, and G. Comsa, Appl. Phys. A: Mater. Sci. Process. **61**, 455 (1995).
[36] J. W. Evans and M. C. Bartelt, in *Morphological Organization in Epitaxial Growth and Removal*, edited by Z. Zhang and M. G. Lagally (World Scientific, Singapore, 1998), p. 50.